SAE INTERNATIONAL®

Implementation of a Rotary Engine (Wankel Engine) in a CFD Simulation Tool with Special Emphasis on Combustion and Flow Phenomena

2015-01-0382

Published 04/14/2015

Johann Spreitzer, Felix Zahradnik, and Bernhard Geringer

CITATION: Spreitzer, J., Zahradnik, F., and Geringer, B., "Implementation of a Rotary Engine (Wankel Engine) in a CFD Simulation Tool with Special Emphasis on Combustion and Flow Phenomena," SAE Technical Paper 2015-01-0382, 2015, doi:10.4271/2015-01-0382.

Copyright © 2015 SAE International

Abstract

This paper describes the development of a comprehensive simulation environment for investigations of gas-dynamic processes and combustion phenomena in rotary engines, conducted by the *Austrian Institute for Powertrains and Automotive Technology* of the *Vienna University of Technology*. In this connection, proven, commercially available engine cycle calculation Software-Tools have been used.

For this, a rotary engine test bench has been established. As analysis tools, in addition to the traditional acquisition of the emitted engine torque, various pressures and temperatures, the recording of the pressure profile (combustion analysis measurement system) in the combustion chamber, as well as in the intake and exhaust ports, were used. The data of the test bench were used to develop and validate the methodology for the simulation tools.

The focus in this paper is the development of a CFD (computational fluid dynamics) model with the software *Converge* from *Convergent Science, Inc.* In close cooperation with *Convergent Science, Inc.*, a functioning basic Wankel model was developed. Using this model, it was possible to monitor and analyze the gas flow and the combustion processes in the three combustion chambers simultaneously.

To calculate the combustion, the *SAGE* module was used. This is a predictive combustion model that is based on the chemical reaction mechanism of the respective fuels. Therefore, a combustion reactor was constructed and the flame propagation was analyzed in detail (Combustion analysis and High-Speed-Camera). Thus, the numerical model could be adjusted and optimized.

Introduction

The Wankel engine has not established itself in wide areas of application in the automotive industry. The only OEM that used the rotary engine for a long time was the *Mazda Motor Corp.* Currently, however, there is no vehicle available from this company that is only powered by a rotary engine. Nevertheless, the Wankel still offers in other application areas plenty of advantages. In most cases, these are simple flight or motorsports applications e.g. the power unit for the gliders from *Alexander Schleicher GmbH & Co Segelflugzeugbau* [1] and drones of the *Schiebel Corp.* [2]. On the motorsport side, the Wankel engine of the kart manufacturer *AIXRO GmbH* [3] must be mentioned. One of the best known and very active supporters of the Wankel philosophy is the *Austro Engine GmbH* [4] from Wiener Neustadt, which also was a research partner for the present investigations at the *Vienna University of Technology*.

In recent years, driven by the progressive electrification of the automotive powertrain, there have been new applications for the Wankel engine also in the automotive industry. Especially due to the Wankel specific advantages such as simplicity, compactness, light weight, low vibration and high efficiency, this engine concept also increases as a range extender. A well-known representative is the 2012 presented prototype in the *A1 e-tron* from the *Audi AG* [5]. This range extender vehicle (REX) uses a Wankel engine to recharge the vehicle batteries while driving and therefore the cruising range is increased. The REX-module comes from *AVL List GmbH* [6]. Similar experiments have also been done by *FEV* in cooperation with *Fiat* [7] and *Mazda Motor Corp.* However even this Wankel engine application has not managed the leap into production [8].

Due to the small numbers of items and low market volume it is difficult for manufacturers to advance the development of this technology. For this purpose, a modern simulation tool is presented in this work. In general, the simulation of engine processes has the advantage that optimization or estimation of a concept can be achieved faster and with lower costs.

This present work, on the one hand, builds up and validates an appropriate development environment for Wankel engines and, on the other hand, converts the knowledge into general statements for the present engine type. In addition, to show the greatest weaknesses of the Wankel engine, an efficiency analysis has been conducted. The used CFD simulation (*Converge*, der *Convergent Science Corp.* [9]) is primarily a consideration of the flow processes in the combustion chamber and to secure the gained knowledge.

The Wankel Engine

The heart of the rotary engine is formed by a triangular piston (rotor) and an eccentric shaft (ES). These two components are the only moving parts of this engine concept. The combustion chamber is bounded peripherally by a trochoidal housing contour and laterally by shallow levels. The rotor is guided by the eccentric shaft and two gearwheels on a circular path. The rotor attached to the internal gear engages in the plate mounted on the pinion of one of the two side windows. This ensures that the rotor center always revolves with the eccentricity e. Each piston rotation equals three revolutions of the eccentric shaft, due to the kinematics [10].

Principle of Operation

Figure 1 illustrates the principle of the Wankel operation mode. It is similar to the common four strokes known from the reciprocating engine. The first phase is the suction. The suction is released from the rotor so that the air can flow into the intake. For this purpose, there are no valves necessary comparable, because the rotor opens the port similar to the two-stroke piston engine. In the second cycle, the trailing edge of the rotor closes the inlet port and the charge can now be compressed. In the case of a direct-injection rotary engine, the fuel is also injected into this stroke. In the next step, the ignition of the compressed mixture takes place and results in expansion of the load. In this phase, the energy of the mechanical work released to rotate the rotor continues. In the fourth and final stroke, the rotor opens the outlet port and the burned gas can be ejected. This process takes place at all three piston surfaces, offset by 360°[EA] or 720°[EA].

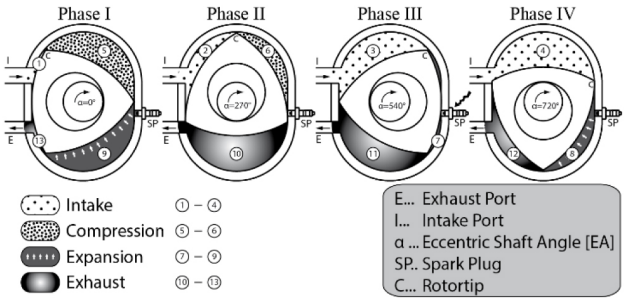


Figure 1. Principle of operation

As with the conventional reciprocating engine, four piston positions are defined as dead center explained in Figure 2

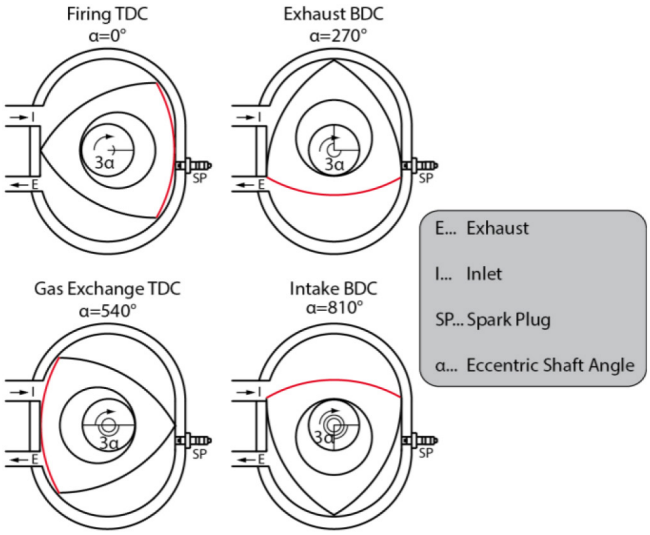


Figure 2. Four dead centers of the rotor in the Wankel engine

The eccentric angle α (EA) is counted from the ignition dead center, as shown in Figure 2. From dead center to dead center, the piston rotates 90°, the eccentric shaft is three times faster and rotates 270°. A piston flank reaches after three turns of the eccentric shaft its initial position. Consequently, the relationship between eccentric shaft [°EA] and rotor angle [°RoA] is according to Figure 2.

$$1 * °RoA = 3 * °\mathrm{EA} \tag{1}$$

Nomenclature of the Wankel-Engine-Trochoid

The trochoid is shown in Figure 3.

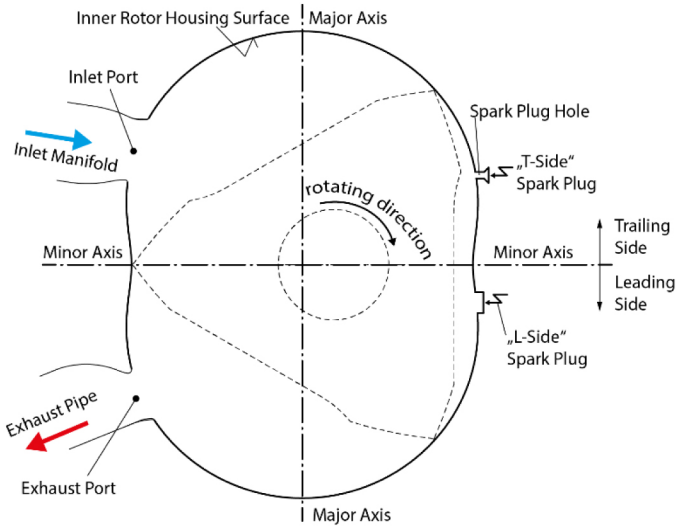


Figure 3. Definition of terms for the trochoid of the Wankel engine similar to the designations in [11]

The individual sections of the trochoid can be divided into individual portions, as shown in Figure 3. Between the two points of the trochoid that are farthest apart, the “major axis” is defined. Between the two points lying most closely together, the “minor axis” is defined.

Pros & Cons

Even if the Wankel engine could not compete with the reciprocating engine in the automotive industry, whether for economic reasons [12], or for technical reasons, it also boasts large advantages over the conventional powertrains in certain subsectors.

Pros:

- good NVH behavior (low vibrations, complete mass balance possible, …)
- compact design (no valve train necessary, …)
- less friction losses
- specific performance (good weight and volume to performance ratio, …)

Cons:

- worse thermal efficiency (crescent-shaped combustion chamber contour, surface-volume ratio)
- higher fuel and oil consumption
- higher production costs
- high position of power dissipating shaft
- compression-ignition engines only with great technical effort (e.g., Rolls Royce)

A detailed overview of the advantages and disadvantages of the Wankel technology is given in [13]. Table 1 highlights the main advantages and disadvantages of the Wankel technology over a conventional reciprocating engine.

Table 1. Advantages and disadvantages of the Wankel engine over the conventional reciprocating engine

criteria		advantages and disadvantages over conventional reciprocating engine
comfort		+ (vibrations), - (noise in the case of outlet in the trochoid)
costs		-
space		+
weight		+
consumption		-
emissions	HC	-
	NOx	+

Testbench & Engine

In the course of the present work, an engine was built up on an engine test bench at the *Institute for Powertrains and Automotive Technology (IFA)* at the *Technical University of Vienna* in cooperation with *Austro Engine GmbH*. This serves the basis for the subsequent investigations.

Experimental Engine

The test engine is a ball bearing one-disk prototype Wankel engine of *Austro Engine GmbH* with electronic intake manifold injection. The technical data are summarized in Table 2. The rotor housing is water-cooled and the engine has two spark plugs positioned parallel after the short axis (2 “L-Side” plugs).

Table 2. Technical date of the test engine

rotor	1
inlet	in the trochoid
outlet	in the trochoid
chamber volume [cm^3]	404
width [cm]	7.44
k-factor[1]	6.3
compression ratio	9.6
power [kW]	35 at 6000 rpm
fuel mixture generation	electronic controlled “semi“-direct injection
# spark plug/ position	2/ parallel
position spark plugs	10 mm after minor axis
bearing	ball bearing
crankcase cooling and lubrication	air/ oil mixture
housing cooling	water

The term “semi”-direct injection is characterized by *Mazda Motor Corp*. [14]. In this case, the injection valve in the intake manifold is positioned so that the fuel is injected directly into the combustion chamber. Because the injector is located in the intake manifold and not directly in the combustion chamber, this arrangement is referred to “semi”-direct injection.

1. The ratio of the distance from piston to piston edge midpoint R and the eccentricity e is defined as k-factor. This is significant for the geometric properties of the trochoid. In addition to other values, it determines the ideal compression ε and hence the surface / volume ratio of the combustion chamber.

Engine Testbench

The test engine was mounted on a test bench with dynamometer. For the test mode, a plenum with a power greater volume, compared to the chamber volume of the engine, was installed before the engine intake manifold. This allowed, on the one hand, investigating the effect of the resonance charging and, on the other hand, measuring the air mass. The engine was completely pressure indicated. Beside the piezoresistive pressure sensors in the inlet and outlet ports, there were piezoelectric pressure sensors over the circumference of the combustion chamber. In addition, a full emission analysis of the exhaust gas was conducted. A schematic overview of the entire test bench is shown in Figure 4.

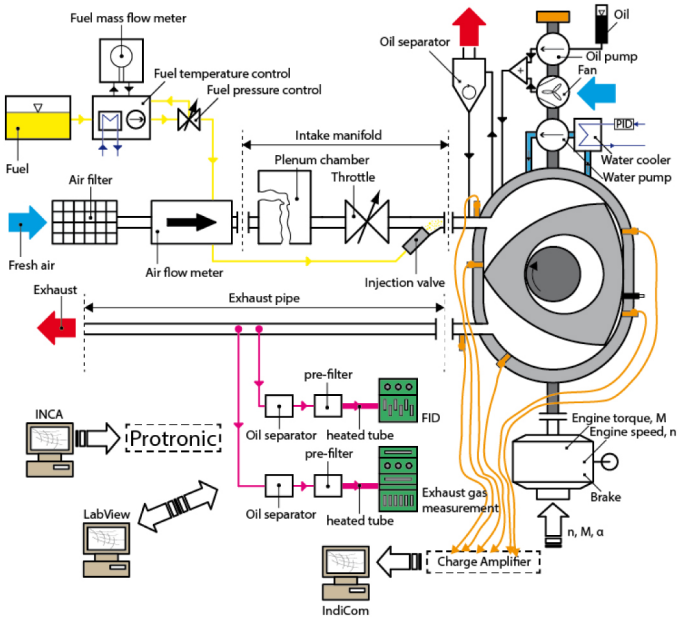


Figure 4. Schematic overview of the entire test bench

Using a CFD Simulation Model for the Wankel Engine

In the course of this research, a CFD simulation model was constructed to give a unique insight into the flow conditions within the Wankel engine. The big challenge was that only very few efforts in the field of CFD simulation have been done in the past with the Wankel engine, compared to the conventional reciprocating engine. Some published work [15], [16], [17] and [18] have mainly dealt with the creation of program codes and the subsequent analysis of the flow phenomena in the combustion chamber. Most of this work comes from the early days of CFD simulation. Recently published work, such as [19], [20], [21], [22] and [23] have used modern CFD tools, but these usually considered only one combustion chamber by itself. Many other studies had no real engine at the test bench to compare the results in relation to measured values.

Special Features when Modeling a Wankel Engine

In order to obtain reproducible results, always 2160 °EA (i.e., six combustions, whereby the first two, either poorly ignite or do not ignite at all due to the start of the simulation at FTDC) were simulated. As boundary conditions, such as at the inletport and outletport values, from the testbench were used. In order to understand which requirements are imposed on a simulation tool for a Wankel engine, some considerations:

Gas Exchange

Since 1940, there are common parameters to DIN ISO for the gas exchange. These also find their application for the Wankel engine. The distribution of the mass during the gas exchange is shown schematically in Figure 5. This is valid for both naturally aspirated as well as supercharged engines. The influence of the leakage is neglected in this analysis.

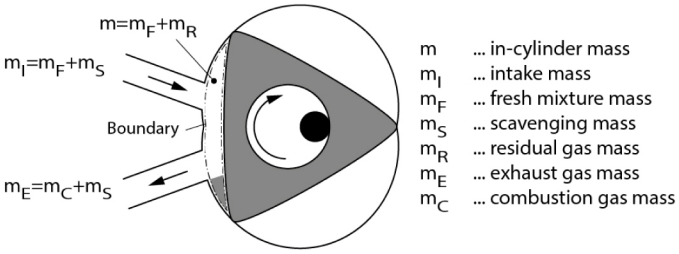


Figure 5. Schematic distribution of the mass during the charge cycle in the Wankel engine. (To compare with the convention reciprocating engine, see [24])

The incoming intake air mass m_I is the total delivered air/ fuel mixture during a charge cycle. For air-aspirating engines (with direct injection) m_I corresponds equal to the intake air mass m_a, for engines with premixtured charge, there is also the added fuel m_f mass to consider. Furthermore m_I equals the remaining fresh charge m_F in the cylinder and the mass m_S not participating by the combustion, flowing during the overlap phase directly into the outlet. In the chamber, the fresh intake charge m_F and the remaining or remitted residual gas m_R from the exhaust, which flows from the trailing chamber, form the total charge mass m. The exhaust gas mass m_E is composed of the combustion gas mass m_C and the mass m_S which flows during the overlap phase directly into the outlet. Thus, the following expressions and dependencies are obtained for the charge masses defined above:

- Air/ Fuel-Mixture aspirating

$$m_a + m_f = m_I = m_F + m_S \tag{1}$$

- Air aspirating

$$m_a = m_I = m_F + m_S \tag{2}$$

The specifics of the charge cycle at using Wankel engine result from the combination of the four-stroke principle and the port control. In addition to the classic gas exchange, there is a special effect on a Wankel engine with inlet and outlet ports in the trochoid, shown in Figure 6. During the opening and closing of the inlet and outlet ports, two combustion chambers are always in direct communication with each other. This part of the charge cycle is referred to an “enhanced gas exchange”. The direct connection of the combustion chambers, as described above, requires an adaptation of the valid assumptions for reciprocating engines. Figure 6 shows a schematic diagram of the mass movements while closing the outlet port. Contemplation is based on chamber 1 (index “I”). The mass which flows from the trailing chamber (II) in the previous chamber (I) is denoted by m_{STC}. Similarly to this, the closing of the inlet port was modeled.

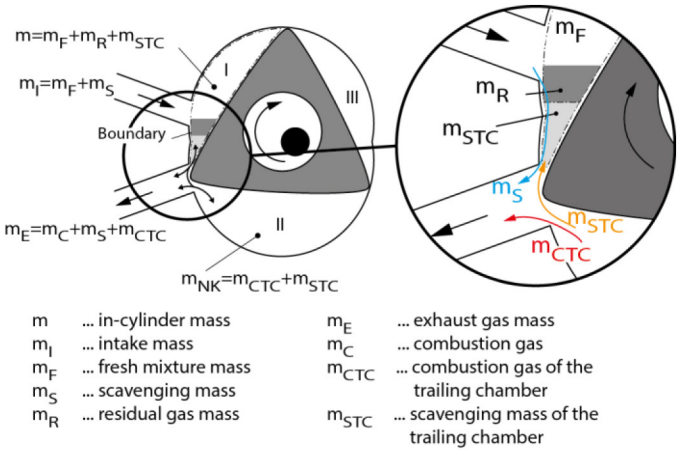


Figure 6. Principle of the mass movements at sliding over the outlet port (chamber I)

Combustion

The model is based on the thermal equation of state and the conservation laws for mass and energy explained in Figure 7.

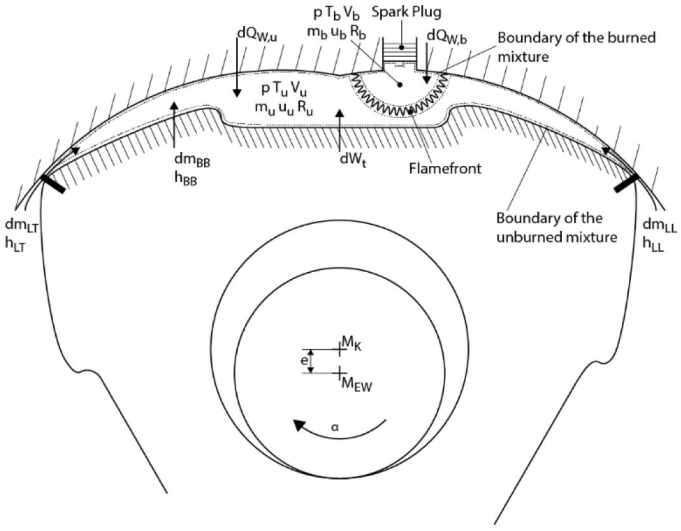


Figure 7. Scheme of the thermodynamic model for a homogeneously operated SI Wankel engine with separated zones of burned and unburned mixture by the flamefront.

Starting with the first law of thermodynamics, neglecting the kinetic energy, we obtain the following for the energy equation (conservation of energy) during the combustion process in an air/ fuel mixture aspirating engine:

$$\frac{dE_u}{dt} = \frac{dU_u}{dt} = \frac{dQ_{W,u}}{dt} - p * \frac{dV_u}{dt} + \frac{dm_{L,u}}{dt} * h_{L,u} \tag{3}$$

$$\frac{dE_b}{dt} = \frac{dU_b}{dt} = \frac{dQ_{W,b}}{dt} - p * \frac{dV_b}{dt} + \frac{dm_{L,b}}{dt} * h_{L,b} \tag{4}$$

With reference to the thermal state equation:

$$p * V_u = m_u * R_u * T_u \tag{5}$$

$$p * V_b = m_b * R_b * T_b \tag{6}$$

and the continuity equation (conservation of mass):

$$\frac{dm_{ent}}{dt} = \frac{dm_u}{dt} + \frac{dm_b}{dt} + \frac{dm_L}{dt} \tag{7}$$

the differential equations of first order with a known combustion process dm_b/dt and known wall heat losses dQ_W/dt can be solved.

The indices *u* and *b* are the unburned and burned mixture, the index *ent* for the entire contents of the cylinder. The index *L* describes the "leakage" loss, which is neglected in the present CFD simulation. To simulate the combustion, *Converge* offers several possibilities. Figure 8 gives an overview of the implemented models.

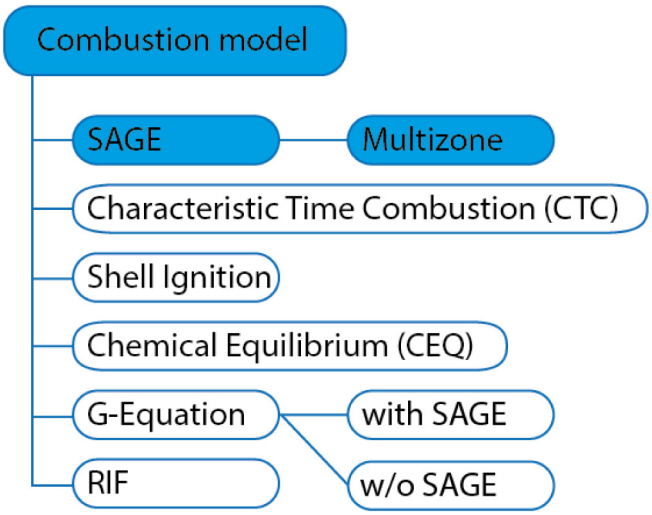


Figure 8. Overview of the implemented models in CONVERGE

In the present work, the *SAGE* model was chosen because it is a general combustion model, which solves the chemical reaction equations during the combustion process in detail. The used *SAGE* model is based on work by *Senecal et al.* [25] and works with a predictive combustion model. The chemical reaction equations are solved in each discretized cell of the fluid. Therefore, the *Converge CVODES* Solver [26], which is integrated into the program package, is used. The chemical reaction equations are defined in *CHEMKIN* format. The reaction mechanism is given as a set of elementary equations to depict a general chemical reaction in detail. The combustion of different fuels can be modeled by changing the reaction mechanism. For the conducted simulation, the single-component fuel Isooktan (IC8H18) was chosen. This fuel comprises 69 individual reaction equations and is frequently used in simulations representative of Gasoline. The reaction mechanism was published and validated in *Jia* [27]. With *SAGE* it is possible to map the ignition directly. For this, a virtual spark plug introduces as much energy in the located cell that it triggers chemical reactions in the affected cells. With the *SAGE*-approach, the software evaluates the mean reaction source term as the reaction source of the mean (which is not valid if the function is non-linear and if the variance is non-zero), so the code always tries to resolve down to sufficiently small cell sizes around the flame front, in order that the species variance is small. This does not scale well with a high Reynolds number, but in this case, the Reynolds number is typically smaller (ca. 5,000 to 50,000). For other cases, a combustion model which accounts for the turbulent fluctuations can be better. For the detailed process of the reaction equations and the process which was integrated into the simulation environment, it is referred to [28] and [29].

As a simplification in the present paper, the air / fuel mixture is assumed to be homogeneous, and the fuel evaporates completely in the calculations.

Validation of the Combustion

To validate the CFD combustion model, and for further investigation with alternative fuels, a combustion reactor (Figure 9. Combustion reactor) was built up. At the same time, a CFD simulation of the combustion reactor was set up to validate the simulation suitability. The results show, for the first shot, very good compatibility and allow reliable statements concerning trends. A detailed tuning of the simulation model (*CHEMKIN* reactions) is part of ongoing research at *IFA*.

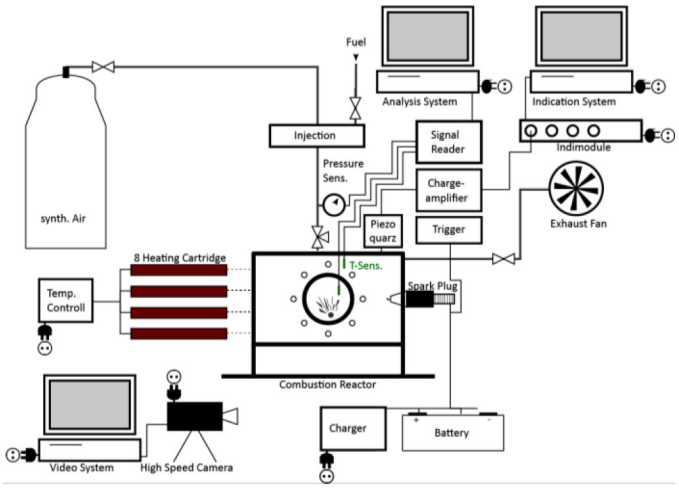


Figure 9. Combustion reactor to validate the CFD combustion model

Generate the Mesh

The flow simulation in the Wankel engine is very special because of the complex movement of the rotor and the strong alteration or distortion of the chamber geometry during the power stroke. In addition, the combustion chambers interact with each other, as explained in the previous chapters. Consequently, the objective of a comprehensive CFD simulation of the flow processes in the Wankel engine is not only the image of a single combustion chamber but also the simultaneous consideration of all three combustion chambers.

To this, *Converge* of *Convergent Science, Inc.* performs an automatic generating mesh during the rotations. The calculated generated mesh, cut through the median plane of the engine, is shown in various positions of the rotor in Figure 10.

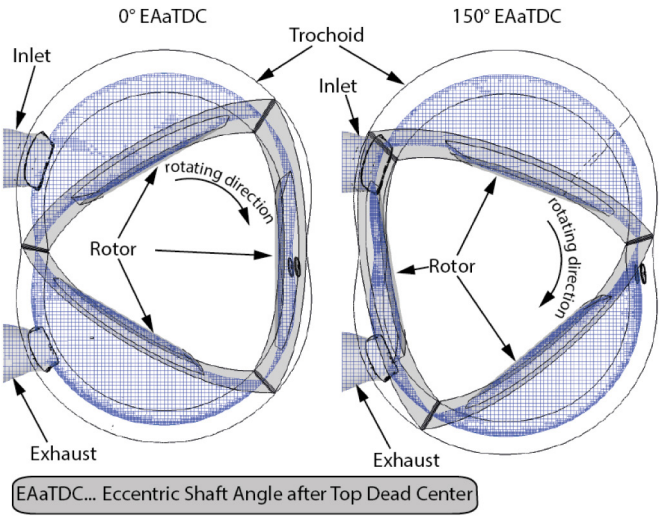


Figure 10. Automatically calculated and generated mesh, cut through the median plane of the engine for two different rotor positions.

Validation of the CFD Model

Using the comparison of the indicated (measured) values and with the CFD simulation calculated values, the pattern quality is shown. Figure 11 shows a comparison between the calculated pressure profile and the pressure profile measured on the testbed in the combustion chamber.

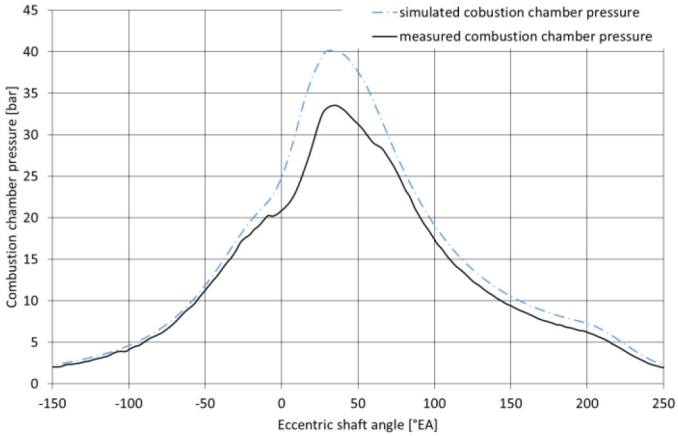


Figure 11. Comparison of the CFD simulation and the measured pressure profile in the combustion chamber at WOT and engine speed of 6000 rpm, ignition timing at −18 ° EAaTDC

In the CFD model, the leakage through the sealing strips was neglected. An implementation of these complex processes is currently in progress. The interaction between the combustion chambers during the sweep of the inletport and outletport and the spark plug hole is considered in this simulation. As expected, the resulting pressure profile from the CFD simulation is higher than the measured one. Nevertheless, the position of the maximum pressure and the gradient is sufficiently characterized in order to assess the combustion properties and valuate different piston geometries based on the CFD simulation. Figure 12 shows the comparison of the results from the simulation and calculated Heat Release Rate.

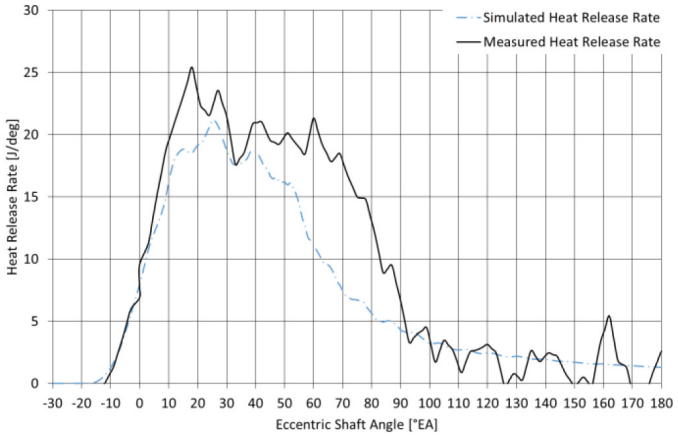


Figure 12. Comparison of the CFD simulation and the measured Heat Release Rate in the combustion chamber at WOT and engine speed of 6000 rpm, ignition timing at −18 ° EAaTDC

This demonstrates the protracted course of combustion with two local maxima, which is characteristic for the Wankel engine. The combustion in the simulation occurs faster than in the measurements. This effect is most likely due to the increased level of pressure in the combustion chamber and the different fuels used. isooctane in the simulation, ROZ95 on the test bench.

In addition to the validation of the quality of the combustion, the flow fields in the combustion chamber are shown in Figure 13 and compared to two in the literature [21] and [23] published simulation results.

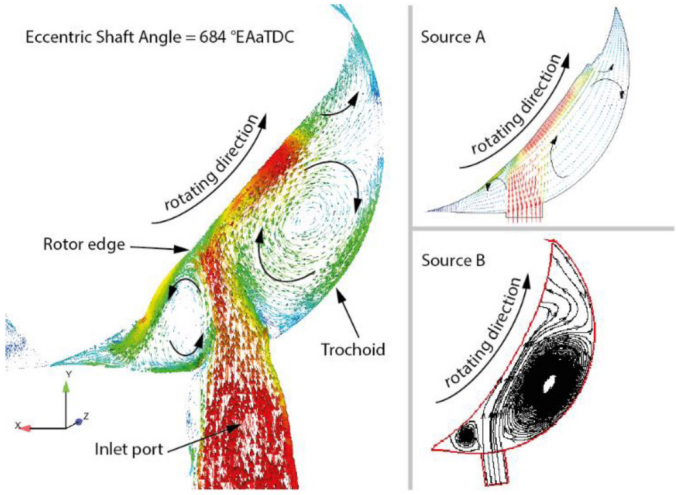


Figure 13. Flow fields in the combustion chamber and comparison with two results from the literature [23] (A) and [21] (B)

In all three cases, very similar flow fields are formed. All three results are from numerical simulations generated with different simulation tools (Source A: *AVL Fire*, Source B: *Fluent*). On the one hand, an intensive return flow after the inlet port plus a large turbulence in the clockwise direction in the main area of the combustion chamber and, on the other hand, a flow in a rotational direction at the end of the rotor recess.

Analysis of the Combustion and Flow Processes

The following chapter deals with the flow processes in the base engine. Especially the phenomena occur during the gas exchange and the flow conditions in the combustion chamber. In particular there are points of particular interest during the initiation of the combustion.

Analyze the Gas Exchange

Figure 14 shows the pressure profile in the combustion chambers and in the inlet and outlet port during one complete revolution of the rotor. As shown, the pressure profile for each combustion chamber is repeated.

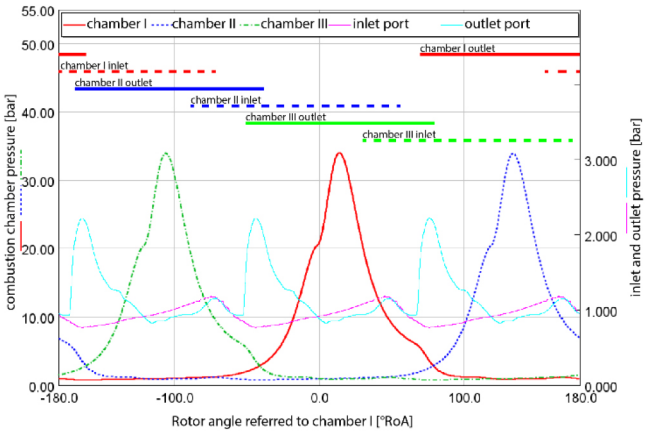


Figure 14. Pressure over one rotor rotation in the combustion chamber and in the inlet and outlet port at WOT and engine speed of 6000 rpm. Opening duration of inlet and outlet port.

As stated above, a combustion chamber in the gas exchange phase is not only with the inlet and outlet port in contact, but also with the adjacent combustion chambers. Considering in detail, as shown in Figure 15, the gas exchange phase for combustion chambers I and III, shows different flow conditions (Phase 1 to Phase 4).

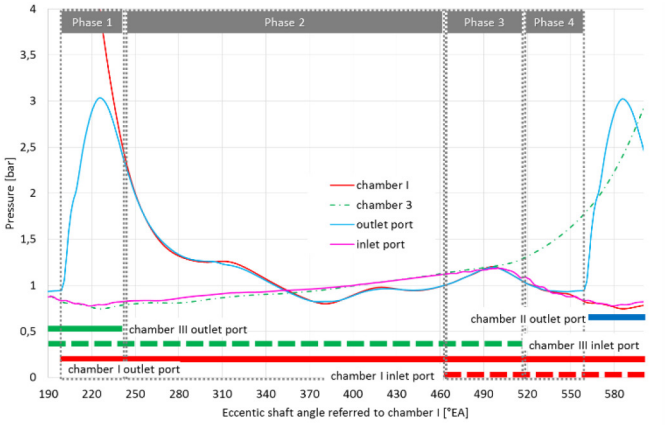


Figure 15. Pressure process in chamber I and III, and in the inlet and outlet port during gas exchange at 6000 rpm and WOT

Taking into account the timing of the inlet and outlet port, as shown in Figure 15, different flow conditions result in the course of the entire gas exchange. These can be divided into four phases, shown schematically in Figure 16.

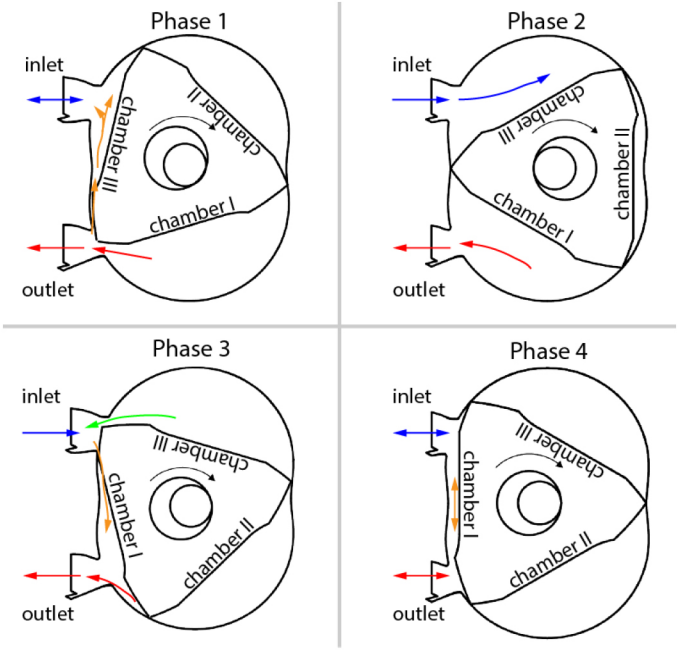


Figure 16. Schematic representation of the four phases of the gas exchange

Detailed explanation of the four phases shown in Figure 16:

- **Phase 1:** The outlet port is opened from the rotor edge and the combustion chamber I and the exhaust starts. Immediately, the same rotor edge begins to close the outlet port for the combustion chamber III. During the entire period, the two combustion chambers are directly connected. As the pressure curve shows, there is an overflow of the burned gas from the combustion chamber I in to the leading combustion chamber III.
- **Phase 2:** Combustion chamber I is only in direct communication with the outlet port and the exhaust gas can be ejected. By pulsation effects in the exhaust manifold, it may result in gas oscillations. The leading combustion chamber III is only in connection with the inlet port and aspirates fresh mixture.
- **Phase 3:** The leading edge of the rotor in combustion chamber I releases the inlet port. Again, the combustion chambers I and III are directly connected, this time through the inlet port. Taking the instantaneous pressure conditions into account, there is an overflow of fresh mixture into the exhaust port. This phenomenon is strongly influenced by the rotor recess. In addition, the leading combustion chamber III pushes fresh mixture back into the intake port.
- **Phase 4:** The leading combustion chamber III is completely sealed and begins with the compression stroke. Combustion chamber I is still with the inlet and outlet port in communication. At this point the inlet and outlet pressure are almost identical. There is a movement of the mass because of the flow field dominated by the rotor rotation.

Similar flow phenomena could be seen in [30] and correlating to the results of the CFD simulations shown in Figure 17.

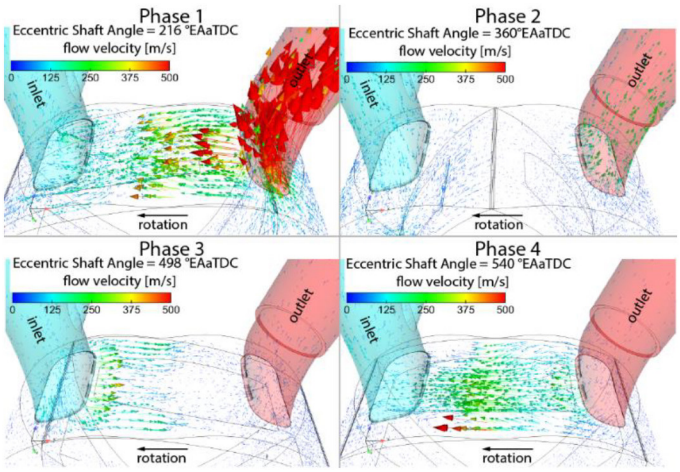


Figure 17. Results of the CFD simulation of the gas exchange at WOT and engine speed of 6000 rpm

Of particular interest are the results from Phase 4: Driven by the rotor movement in this phase, the mass flows from the outlet to the inlet port. There is a significant influence of the design and length of the intake and exhaust manifold, but also the interplay between the rotor, inlet and outlet ports contour plays a crucial role on the overall gas exchange. Looking at the intake and compression process, in the period from the exhaust port closed until ignition, the following flow fields are generated. The cut on Figure 18 runs through the median plane of the engine, parallel to the side walls. The picture is taken immediately after the exhaust port is closed by the trailing edge of the rotor.

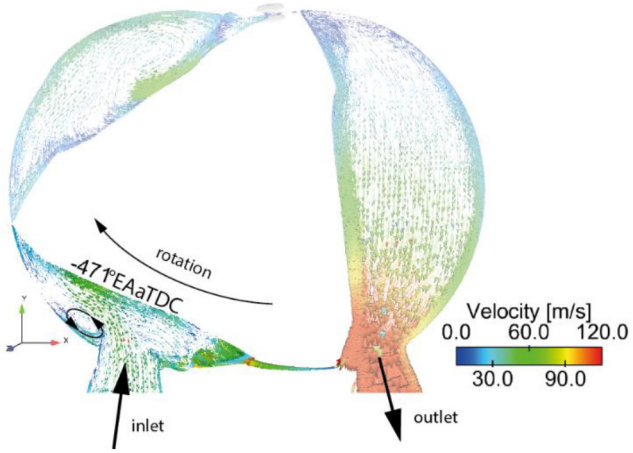


Figure 18. Flow field direct after "outlet-closed"

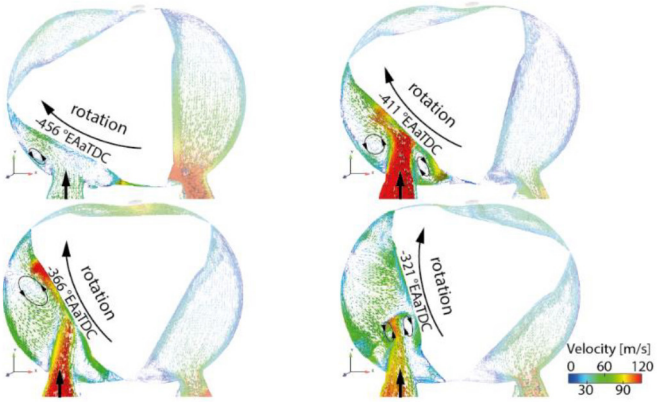


Figure 19. Flow field during the intake

Consequently, immediately after the inlet port opening, fresh mixture is aspirated into the combustion chamber and turbulences occur. The rest of the intake process till "intake closing" is shown in Figure 19.

During the intake process, a free jet is formed which breaks up into small turbulences towards the end when the suction effect of the rotor decreases. Figure 20 shows the flow field during "intake closing" and the compression.

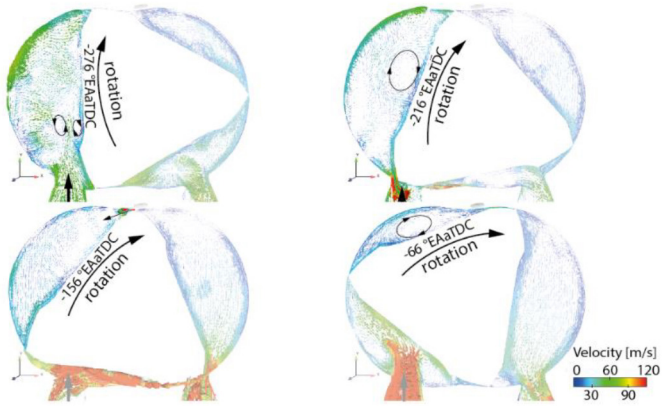


Figure 20. Flow field during the compression till −66°EAaTDC

The smaller vortices, which were initiated by the free jet, slowly disintegrate. Subsequently, at the end of "intake closing", there is an intense return flow in direction to the inlet port. The third picture of Figure 20 shows the influence of the sweep over the spark plug hole of the leading edge on the rotor in the combustion chamber. A pulse is initiated and creates a turbulence in the combustion chamber. The further process to the FTDC is illustrated in Figure 21

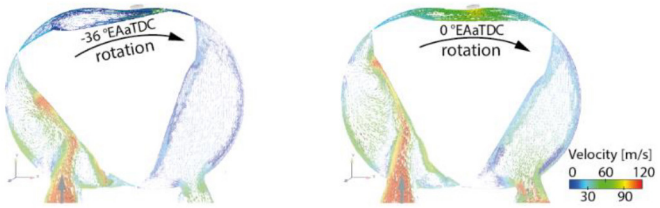


Figure 21. Flow filed at the end of the compression till the TDC

The turbulence decays in a directed flow in the direction of rotation and thus produces an intense flow field, which has a decisive influence on the combustion characteristics of the Wankel engine.

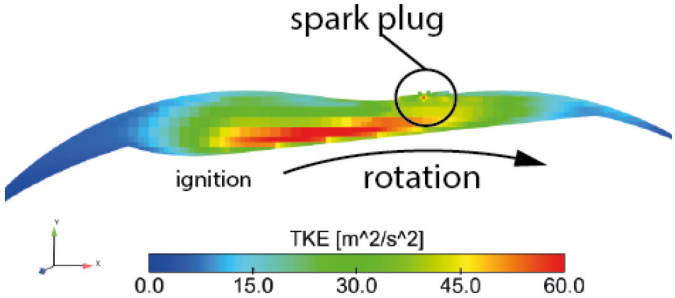


Figure 22. Distribution of turbulent kinetic energy in the combustion chamber

With the help of the CFD simulation, the analysis of the turbulent kinetic energy (TKE) in the vicinity of the spark plug, at the ignition timing, is possible as shown in Figure 22. Lord remarked in [31] that the turbulence has a positive influence on the development of the

turbulent flame front. The author could confirm, on the basis of experimental studies, a faster growth of the initial flame, partly because of high turbulence.

The turbulent kinetic energy is about 30 to 45 m^2/s^2 in the vicinity of the spark plug.

Analyze the Combustion

The combustion process in the rotary engine is the crucial point to reduce the losses of this engine concept. The protracted and retarded combustion results in very high efficiency losses. As the investigations determined, a movement of the center of heat release to the optimal range can hardly succeed with the investigated combustion chamber configuration. Based on the investigations on the engine test bench, Figure 23 shows that it is not possible to shift the center of heat release less than 30° EA, even with a very early ignition timing. The burning duration drastically increases with an early ignition timing.

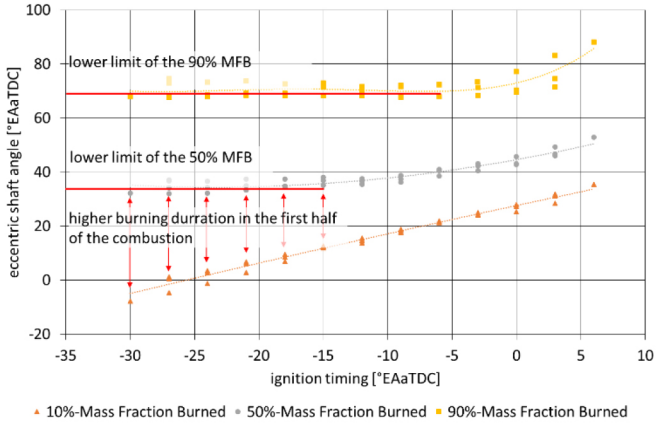


Figure 23. Influence of an early ignition timing to the MFB at WOT, engine speed =3000 rpm with λ = 0.9

This phenomenon occurs in all operating points of the engine, as Figure 24 shows.

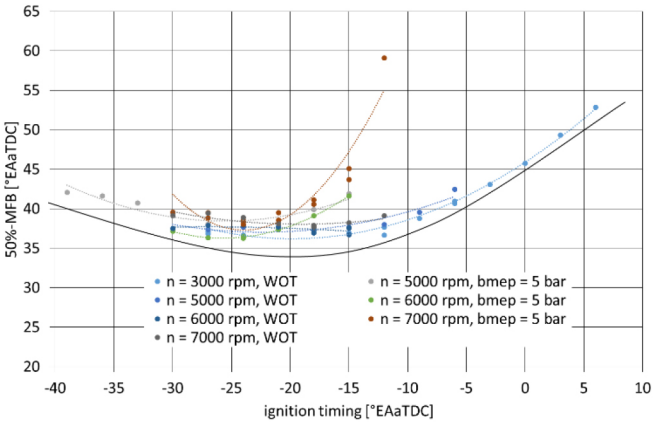


Figure 24. Center of heat release (50%-MFB) on different operating points

As can be seen in Figure 20, a limit (black line) defines the reachable optimum. It is not possible to shift the 50% -center of heat release earlier than 35 °[EAaTDC]. With increasing early ignition timing, the position of the center of heat release increases again. Apparent is the fact that with increasing load and revolutions, the earliest location of the center of heat release shifts earlier °[EAaTDC]. This indicates a lack of turbulence as already observed in [28] and results in a slow combustion process. The reason for the characteristics described above is shown in Figure 25, looking at the heat release of the individual variations of ignition timing (shown in Figure 23).

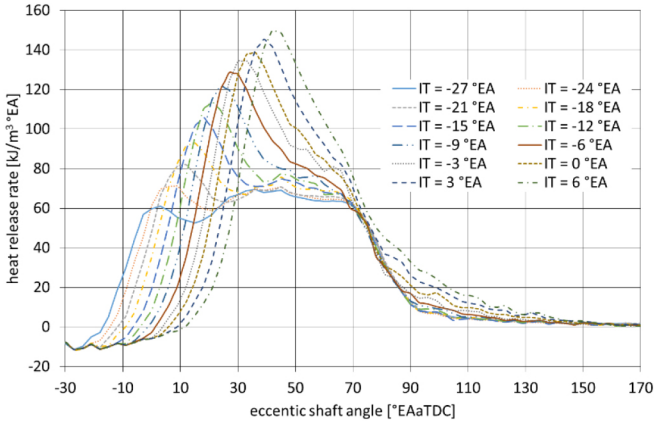


Figure 25. Dependency of the heat release rate by the ignition timing (IT) at 3000 rpm, WOT, λ = 0.9

By adjusting the combustion initiation to an early °EA, it is possible to move forward the start of combustion forward. However, it appears as shown in the heat release that the flame is not able to spread freely. That fact is shown even clearer by considering the heat release in Figure 26.

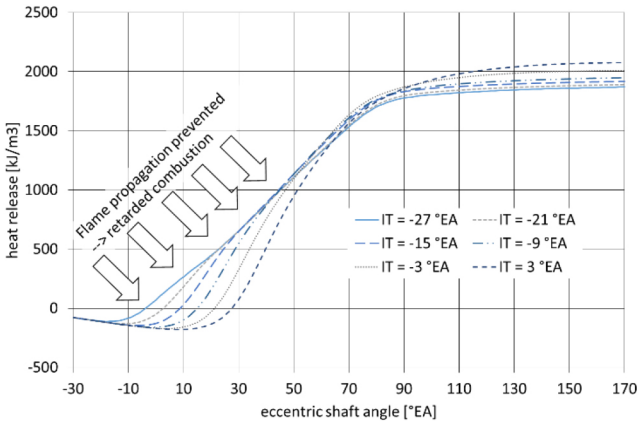


Figure 26. Heat release dependency of the ignition timing [IT] at 3000 rpm, WOT, λ = 0.9

As can be seen in Figure 26 an early ignition leads to a protracted burning duration and does not improve the efficiency. The reason for this combustion characteristic results from the flow phenomena in the combustion chamber at the ignition dead center, commonly referred to “squish flow”. The characteristic of the Wankel engine squish flow is created due to the movement of the combustion chamber with the rotor. The entire mixture in the combustion chamber moves over the entire trochoid from the intake to the exhaust stroke. The shape of the combustion chamber changes from almost semicircular to crescent-shaped. Figure 27 shows the various stages of the combustion chamber shape from 90°RoA before FTDC to FTDC.

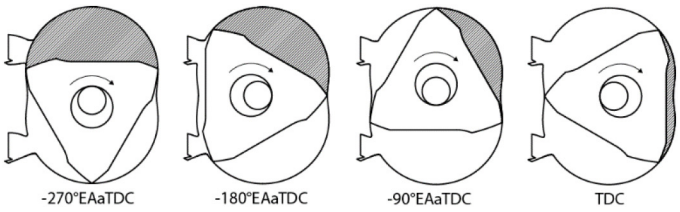


Figure 27. Deformation of the combustion chamber depending on the eccentric shaft angle till ignition position

Looking at the trailing side of the combustion chamber in the period from just before FTDC until just after FTDC, it can be shown that this area becomes narrower, until it finally dissolves completely. The majority of the unburned mixture in this area needs to be replaced at this time in the leading part of the combustion chamber. This produces a strong flow from the trailing to the leading side, as shown schematically in Figure 28.

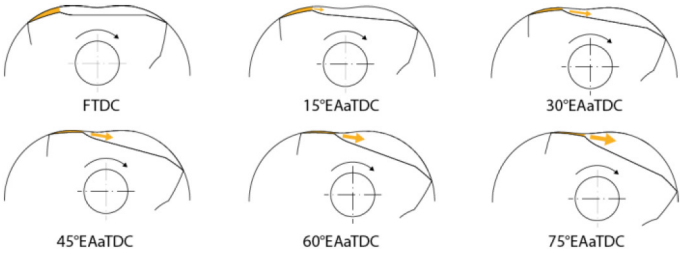


Figure 28. Reason for the development of the squish flow

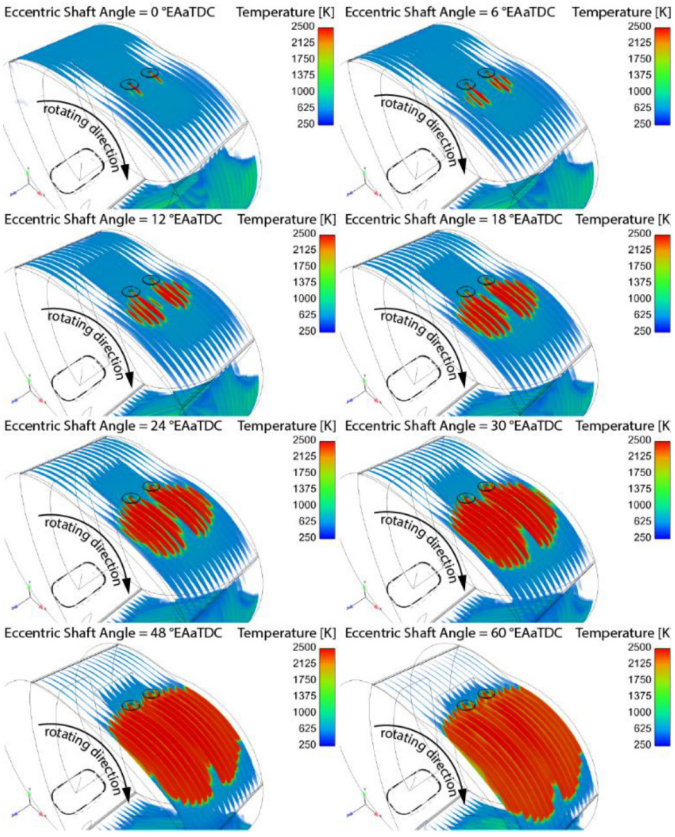


Figure 29. Temperature profile in the combustion chamber from 0°EAaTDC to 60°EAaTDC at engine speed of 6000 rpm, WOT, ignition timing −6°EAaTDC

Due to the squish flow, the flame propagation is retarded [11] against the direction of rotation of the rotor and intensifies the wall heat flux. As proved, the remaining unburned mixture combusts until it has escaped from the trailing part of the combustion chamber. Figure 29 shows the process described above with reference to the CFD simulation. The flame spreads primarily in the same direction as the rotation of the rotor. Similar results are shown in [31] and [32] based on test bench measurements and in [16] with the help of CFD simulation. The penetration in the opposite direction happens very late because of the pronounced squish flow.

The reason is that the gas velocities of the squish flow in the region of the flame formation move at about 70 to 180 m/s (see Figure 30), while turbulent flame front speed as a function of pressure, temperature and turbulence in the combustion chamber of a conventional SI reciprocating engine has a one power lower value, shown in [33], [34], [35], [36] and [37].

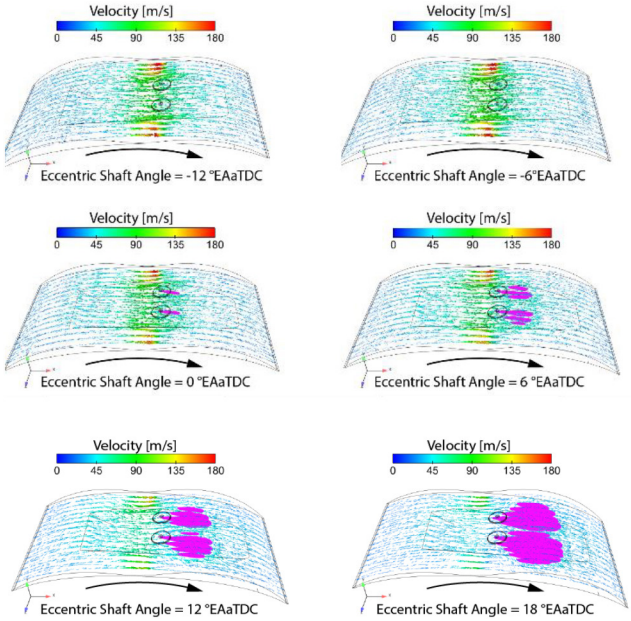


Figure 30. Flowfield from −12°EAaTDC to 18°EAaTDC of the investigated Engine at 6000 rpm, FOT, ignition timing = −6°EAaTDC

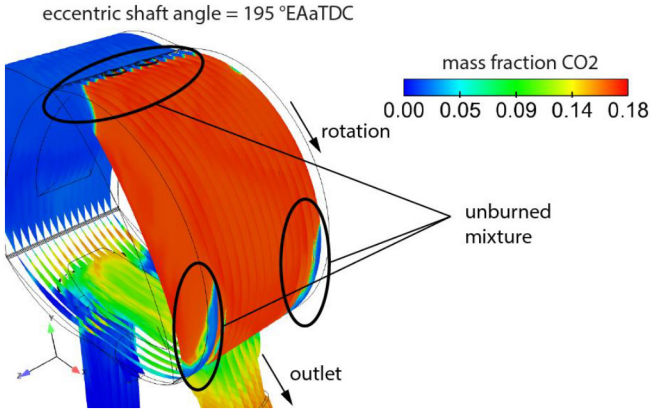


Figure 31. Flame propagation figured with CO_2 mass fraction, before "exhaust port opens", engine speed 6000 rpm, WOT, ignition timing = −6°EAaTDC

The formation of an intensive squish flow in the region of the minor axis between the rotor crown and the trochoid, results as described above, in high flow velocity thus preventing the flame propagation against the rotating direction of the rotor. Another challenge for the Wankel engine is the incomplete combustion of the air/ fuel mixture,

due to the unfavorable shape of the combustion chamber and the relatively high surface to volume ratio and the low turbulence at the time of the start of combustion. Figure 31 illustrates with reference to the performed CFD simulation of the flame propagation immediately before the opening of the outlet port in the investigated Wankel engine.

As shown, the flame front in the investigated base engine does not reach the leading corner. The trailing side is recessed over the entire width of the combustion. The phenomenon shown in Figure 31 is responsible, amongst other circumstances, for the high HC emissions of the Wankel engine, as already [38] and [39] revealed. Another cause of HC emissions is the leakage of the sealing strips and the resulting oil combustion.

Loss Analysis

The loss analysis is based on an 1D model of the engine. The used software *GT-Power* comes from *Gamma Technologies, Inc.* [40]. For the loss analysis, a partial ideal motor is used as a base. For this, the wall heat losses in the combustion chamber and all leakages are neglected. In addition, it is assumed that the MBF50 is optimal in the TDC. The burning duration is 0 °EA and represents the theoretical case of the isochoric combustion. In addition, the engine is operated with λ = 1 and the mixture is completely combusted.

The method of the distribution of losses used here is inspired by [41] and is shown in the following formula:

$$\eta_r = \eta_{ideal} - \Delta\eta_g - \Delta\eta_m \tag{8}$$

η_r ... *real efficiency*

η_{ideal} ... *ideal efficiency of the standard cycle*

$\Delta\eta_g$ ... *quality grade* $(= \frac{indicated\ efficiency}{ideal\ efficiency})$

$\Delta\eta_m$ ... *mechanical loss*

The quality grade can be defined as follows:

$$\Delta\eta_g = \Delta\eta_{RC} + \Delta\eta_{Imp} + \Delta\eta_{Comb} + \Delta\eta_{WH} + \Delta\eta_{Leak} + \Delta\eta_{GE} \tag{9}$$

$\Delta\eta_{RC}$ ... *loss due to real charge*

$\Delta\eta_{Imp}$ ... *implementation loss*

$\Delta\eta_{Comb}$ ... *combustion loss*

$\Delta\eta_{WH}$ ... *wall heat loss*

$\Delta\eta_{Leak}$ ... *leakage loss*

$\Delta\eta_{GE}$ ...*gas exchange loss*

The losses are all stated in percentages.

Ideal Reference Cycle

With reference to [42], the loss analysis is based on the constant-volume cycle. Based on the theoretical efficiency of the engine at isochoric combustion, the following formula results:

$$\eta_{ideal} = 1 - \frac{1}{\varepsilon^{\kappa-1}} \tag{10}$$

With the geometric compression ratio of the engine $\varepsilon = 9.65$ and the isentropic exponent $\kappa = 1.4$ as follows:

$$\eta_{ideal} = 59{,}6\%$$

Alternatively, the loss analysis can also be defined on the dynamic compression ratio as:

$$\varepsilon_{dyn} = \frac{V_{dis} + V_{IC}}{V_{IC}} \tag{11}$$

V_{dis} … *displacemnt volume of a chamber*

V_{IC} … *volume of the chamber at "intake close"*

This considers the closing timing of the intake port. Only after this event, can the charge be compressed. On the investigated Wankel engine the ideal efficiency results in:

$$\eta_{ideal,dyn} = 57.4\%$$

In the present analysis η_{ideal} was used as the reference.

Efficiency Loss Due to Real Charge $\Delta\eta_{RC}$

It must be considered that the isentropic exponent κ = 1.4 for pure air was used in the calculation. Due to the real combustion of the mixture, the real polytropic exponent n is lower. This is entirely due to the changes in material properties of the real cylinder charge. Assuming pure air as reference material, these loss can be considerable. By adding fuel into the intake port, these losses even reach higher values [43].

Efficiency Loss Due to Incomplete Combustion $\Delta\eta_{Imp}$

A perfect combustion is achieved if the combustion proceeds to the chemical equilibrium. Especially with an engine operating under stoichiometric, this loss grows strongly. However in stoichiometric or lean combustion, this loss is mostly about 1% [43] for gasoline engines. The determination of incomplete burned fuel is possible, according to [44], based on the measured HC and CO emissions. In this case, however, it is assumed that the influence from the HC emissions caused by the burned engine oil are negligible. This simplification is reasonable for most modern 4-stroke reciprocating piston engines, but it is not permitted for the rotary engine. For the lubrication of the sealing elements, there are significant quantities of engine oil required, which also plays a part in the combustion. In this case, the determination of the fraction of unburned fuel is possible by means of adapting the pressure profile with the help of the measured pressure profile.

Efficiency Loss Due to Combustion Loss $\Delta\eta_{comb}$

The real combustion in the engine is not isochoric and does not take place at TDC. Thus, this loss can be divided into two.

Efficiency loss due to the center of heat release $\Delta\eta_{rCOHR}$

According to [42], it is assumed that the energy conversion takes place isochorically, but not at the TDC, but based on the real position of the MBF50 of combustion.

Efficiency loss due to real heat release $\Delta\eta_{rHR}$

In this step, the real duration and shape of the heat release is considered. In Figure 32, areas that are enclosed between isochoric and real combustion processes are marked. These have to be accumulated and considered as loss.

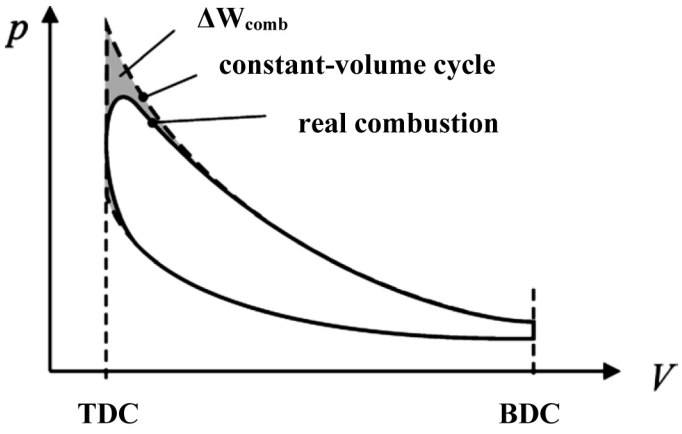


Figure 32. Loss due to real combustion [43]

Efficiency Loss Due to Wall Heat Flux $\Delta\eta_{WH}$

For the determination of the wall heat loss, a wall heat flux model adapted for the rotary engine. The heat transfer coefficient is determined primarily by pressure and temperature in the combustion chamber. In addition, the time when the heat transfer is effected to the combustion chamber should also be mentioned [42].

Efficiency Loss Due to Leakage Loss $\Delta\eta_{Leak}$

These efficiency losses are mostly neglected in loss analysis for conventional reciprocating engines [43]. In rotary engines this may not happen because the leaks in the Wankel engine are one of the weakest points of the engine concept.

The sealing of the combustion chamber on the Wankel engine is based on the same principle as on the reciprocating engine but also with some complicated sealing strips and bolts because cylindrical seals cannot be used. Figure 33 shows a typical sealing system of a Wankel engine. As expected, at the points between the individual sealing parts, inevitably leakage occurs.

On the one hand, combustion gas flows past the sealing and enters the room of the eccentric shaft, similar to the “blow-by” loss in reciprocating engines. On the other hand, it flows into the leading and trailing chamber, depending on the pressure difference. Investigations of Wankel engines have shown that these processes are not negligible in any way.

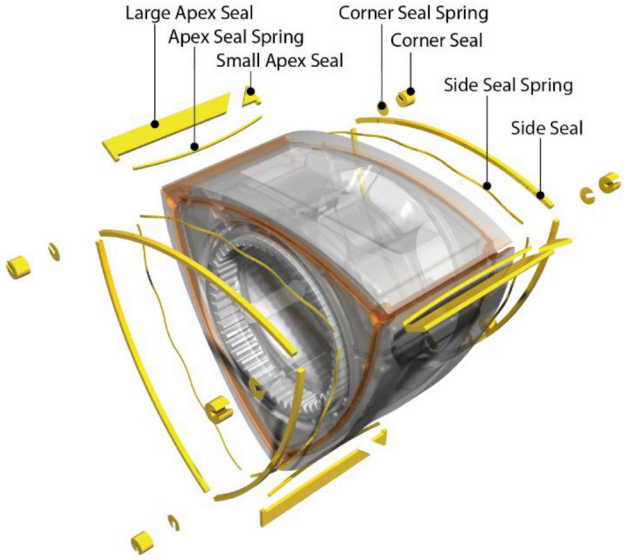


Figure 33. Illustration of the sealing system of a Wankel engine

In principle, the gas has three ways to emanate through different paths from the combustion chamber:

Efficiency loss due to Apex Seals $\Delta\eta_{Leak\ Apex}$

Due to of thermal expansion, a certain clearance between all the seals is necessary. The resulting flow between trochoid and the apex seals is responsible for this loss. The gas can escape through the gap between the apex seal and the trochoid while the apex seal is being lifted from the trochoid, as shown in schematic Figure 34.

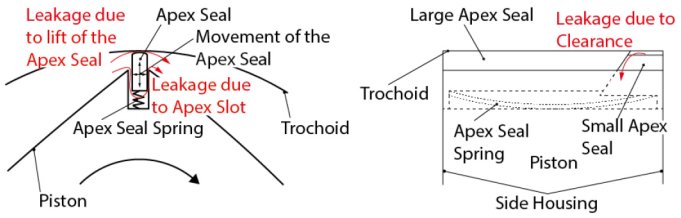


Figure 34. Schematic representation of the leakage losses (exaggerated gaps) via the Apex Seal

Efficiency loss due to leakage via the spark plug hole $\Delta\eta_{Leak\ SH}$

This loss is caused by the apex seal which sweeps over the sparkplug hole. Due to this, a cross-section is released to the adjacent combustion chamber and gas can flow. (see Figure 35)

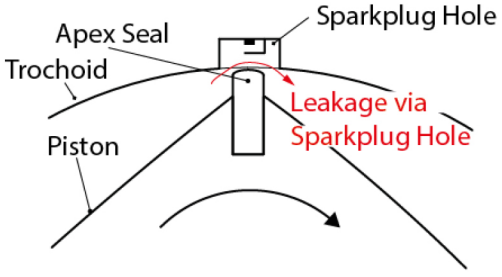


Figure 35. Schematic representation of the leakage losses via the spark plug hole

Efficiency loss due to Side Seals $\Delta\eta_{Leak\ SS}$

The leakage to the eccentric shaft is mainly due to the clearance between the apex seal and corner seal. Furthermore, also the side seal, (i.e., the seal to the housing) can lift and let the burned gas pass via the side seal slot. Figure 36 shows these processes schematically.

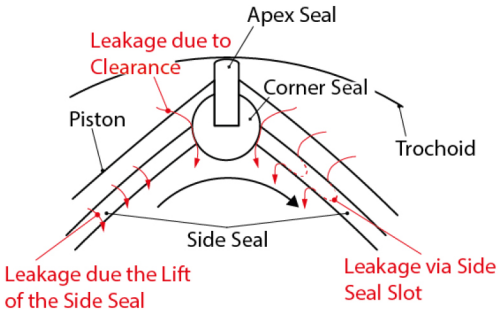


Figure 36. Schematic representation of the leakage losses over the side seals

Efficiency Loss Due to Gas Exchange $\Delta\eta_{GE}$

In order to intake the fresh charge and discharge the burned gas, gas exchange work needs to be done, which is crucial for the gas exchange losses. In quantity-controlled engines, these gas losses increase at part load to a dominant position. Based on the pV diagram, it is possible to determine the necessary gas exchange work.

In summary, the loss analysis shows that the main losses of the Wankel engine result from the protracted and retarded combustion. Consequently, the wall heat losses are lower than expected. An additional potential to improve the efficiency is a proper sealing of the combustion chambers and the correct positioning of the spark plug holes. The mechanical losses, as well as the gas exchange losses, are lower than comparable conventional spark ignition reciprocating engines. The comparison between the investigated Wankel engine and a normally aspirated, throttle-controlled gasoline engine with port fuel injection under full load and high revolutions, is illustrated in Figure 37.

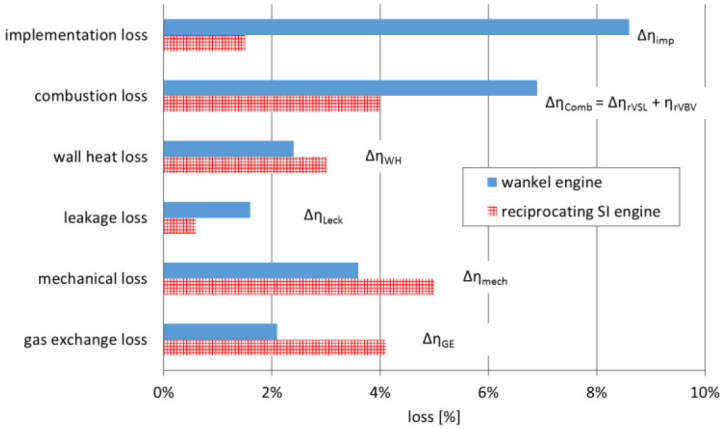


Figure 37. Efficiency differences of the investigated Wankel engine and conventional normally aspirated SI reciprocating engine at high revs and WOT (data from the conventional engine are taken from [45], [43] and [46])

The largest deficits of the Wankel engine can be found in the area of combustion (implementation loss due to incomplete implementation of the fuel $\Delta\eta_{imp}$ and combustion loss $\Delta\eta_{Comb}$) and leakage (leakage loss $\Delta\eta_{Leck}$). The lower wall heat release loss $\Delta\eta_{WH}$, compared to the conventional gasoline engine, results from the late and delayed combustion. The lower mechanical losses $\Delta\eta_{mech}$ and charge exchange losses $\Delta\eta_{GE}$ arise from the port control and consequently, absence of the valve train.

Summary

It is possible to use an existing, commercially available CFD simulation software to representing the procedures in the special case of the Wankel engine in detail. Therefore, with the support of *Convergent Science, Inc.*, an efficient simulation environment can be established. The results of the used simulation tools confirm, on the one hand, the known disadvantages and problems (poor thermal efficiency, high emissions) of this engine concept but, and on the other hand, the Wankel engine could be investigated in an unprecedented analysis depth. Especially the detailed analysis of the efficiency losses and the combustion process reveal new results. Due to other research, it is able, with the help of the developed analysis tools, to confirm the biggest disadvantage of the Wankel engine, the delayed combustion and thereby resulting late position of the center of heat release, in a novel quality. This deficit is based on the massive squish flow, which is generated while sweeping over the FTDC and therefore, the mass flow from the trailing region of the combustion chamber squishes into the leading area of this chamber.

References

1. "Alexander Schleicher GmbH & Co Segelflugzeugbau," [Online]. Available: http://www.alexander-schleicher.de/. [Accessed 23 04 2014].
2. Schiebel Corp., Schiebel - Camcopter S-100 - Unmanned Air System, Wien, Austria: Schiebel Corp., 08/2013.
3. AIXRO GmbH, "Aixro," KaiKaito, [Online]. Available: http://www.aixro.de/. [Accessed 23 04 2014].
4. Austro Engine GmbH, "Austro Engine," roromedia GmbH, [Online]. Available: http://austroengine.at/. [Accessed 23 04 2014].
5. von Maydell M., "Wankelmutig über 250 Kilometer," Auto Motor und Sport, Nr. Heft 15/2012, 20. Juli 2012.
6. Sams T. und Sifferlinger B., "AVL Rotary Range Extender - A Rotary Engine Based Range Extender Concept," in E- Mobility 2013, Graz, 6. Februar 2013.
7. Andert, "KSPG Range Extender mit "FEVcom" Full Engine Vibration Compensation," Spectrum - Technoligie-Highlights aus dem FEV-Arbeitsspektrum, Nr. 49, p. 3, Oktober 2012.
8. Hornig R., "Kippt Audi den Wankelmotor als Reichweitenverlängerer für den A1 e-tron?," Auto Bild, Nr. 11, 2011.
9. Convergent Science Corp., "Convergent Science," [Online]. Available: http://www.convergecfd.com/. [Accessed 23 04 2014].
10. Grohe H. und Russ G., Otto- und Dieselmotoren, Germany: Vogel Buchverlag, 2007, ISBN 978-3-8343-3078-9.
11. Ansdale R. F., Der Wankelmotor - Konstruktion und Wirkungsweise, Stuttgart, Deutschland: Motorbuch Verlag, 1971.
12. Popplow M., Motor ohne Lobby?, Heidelberg: verlag regionalkultur, 2003, ISBN 3-89735-203-6.
13. Kweon C.-B. M., A Review of Heavy Fueled Rotary Engine Combustion Technologies, Maryland, USA: Army Research Laboratory, 2011.

14. Yamaguchi J. K., RX-8 - The Mazda RX-8: World's First 4-door, 4-seat Sports Car Plus Complete Histories of Mazda Rotary Engine Development and Rotary Racing Around the World, 1. Hrsg., Japan: Mazda Motor Corp., 2003, ISBN 4-947659-02-5.
15. Irion C. E. und Mount R. E., Stratified Charge Rotary Engine Critical Technology Enablement Volume I, Wood-Ridge, New Jersey: NASA Contractor Report 189106, 1992.
16. Abraham, J. and Bracco, F., "Comparisons of Computed and Measured Pressure in a Premixed-Charge Natural-Gas-Fueled Rotary Engine," SAE Technical Paper 890671, 1989, doi:10.4271/890671.
17. DeFilippis, M., Hamady, F., Novak, M., and Schock, H., "Effects of Pocket Configuration on the Flow Field in a Rotary Engine Assembly," SAE Technical Paper 920300, 1992, doi:10.4271/920300.
18. Hamai, Y. and Outa, E., "A Two-Dimensional Computer Simulation of Exhaust Gas Behavior Inside a Rotary Engine System," SAE Technical Paper 930681, 1993, doi:10.4271/930681.
19. Berg H. P., Izweik H. T., Poojitganont T. und Antoshkiv O., Anwendung fortschrittlicher Simulationswerkzeuge in der Wankelmotorenentwicklung, BTU Cottbus, Lehrstuhl Verbrennungskraftmaschinen und Flugantriebe: ATZ / MTZ - Konferenz Virtual Powertrain Creation, München, 2006.
20. Berg H. P., Antoshkiv O., Izweik H. T., Poojitganont T. und Himmelberg A., Brennverfahrensentwicklung für eine neuartige Kreiskolbenmotorenfamilie, BTU Cottbus, Lehrstuhl Verbrennungskraftmaschinen und Flugantriebe: ATZ / MTZ - Konferenz Virtual Powertrain Creation, München, 2008.
21. Ma H. L., Kuo C. H. und Chen C. C., Chamber Contour Design and Compression Flow Calculations of Rotary Engine, Department of Mechanical Engineering, National Chung-Hsing University: Journal of C.C.I.T., VOL.39, May, 2010.
22. Wadumesthrige A. A. B., Computational Investigation of Optimal Havy Fuel Direct Injection Spark Ignition in Rotary Engine, Wright State University, 2011.
23. Izweik H. T., CFD Investigations of Mixture Formation, Flow and Combustion For Multi-Fuel Rotary Engine, Dissertation, Cottbus: BTU Cottbus, 2009.
24. Eichlseder H., Klüting M. und Piock W. F., Grundlagen und Technologien des Ottomotors - Der Fahrzeugantrieb, H. List, Hrsg., Wien: Springer-Verlag, 2008, ISBN 978-3-211-25774-6.
25. Senecal, P., Pomraning, E., Richards, K., Briggs, T. et al., "Multi-Dimensional Modeling of Direct-Injection Diesel Spray Liquid Length and Flame Lift-off Length using CFD and Parallel Detailed Chemistry," SAE Technical Paper 2003-01-1043, 2003, doi:10.4271/2003-01-1043.
26. Serban R. und Hindmarsh A. C., CVODES: An ODE Solver with Sensitivity Analysis Capabilities, Livermore, CA, USA: U.S. Department of Energy, Lawrence Livermore National Laboratory, September 2003.
27. Jia M. und Xie M., A chemical kinetics model of iso-octane oxidation for HCCI engines, Dalian, China: Science Direct, Fuel 85 (2006) 2593-2604, 2006.
28. Convergent Science, Inc., Converge 2.1.0 - Theory Manual, Madison, USA: Convergent Science, Inc., 2013.
29. Turns S. R., An Introduction to Combustion, Bratislava: McGraw-Hill, Inc., 1996.
30. Jeng, D., Hsieh, M., Lee, C., and Han, Y., "The Intake and Exhaust Pipe Effect on Rotary Engine Performance," SAE Technical Paper 2013-32-9161, 2013.
31. Yamamoto K., Rotary Engine, Tokyo, Japan: Sankaido Co., Ltd., 1981.
32. Nagao A., Yoshioka S., Ohnishi K. und Tanaka K., Flame Propagation and Knocking in Wankel Rotary Engines, Proc. of Combustion Symposium of JSME, December 1985.
33. Heywood J. B., "Combustion and its Modeling in Spark-Ignition Engines," in The 3rd International Symposium on Diagnostics and Modeling of Combustion in Internal Combustion Engines (COMODIA 1994), Yokohama, Japan, 1994.
34. Samaga, B. and Murthy, B., "On the Problem of Predicting Burning Rates in a Spark Ignition Engine," SAE Technical Paper 750688, 1975, doi:10.4271/750688.
35. Keck J. C., Turbulent Flame Structure And Speed In Spark-Ignition Engines, MA 02139: Massachusetts Institute of Technology Cambridge, 1982.
36. Wirth, M., Keller, P., and Peters, N., "A Flamelet Model for Premixed Turbulent Combustion in SI-Engines," SAE Technical Paper 932646, 1993, doi:10.4271/932646.
37. Metghalchi M. und Keck J. C., Burning Velocities of Mixtures of Air with Methanol, Isooctane, and Indolene at High Pressure and Temperature, New York: Elsevier Science Publishing Co., Inc.;Combustion and Flame 48 (191-120), 1982.
38. Danieli, G., Keck, J., and Heywood, J., "Experimental and Theoretical Analysis of Wankel Engine Performance," SAE Technical Paper 780416, 1978, doi:10.4271/780416.
39. Ohkubo, M., Tashima, S., Shimizu, R., Fuse, S. et al., "Developed Technologies of the New Rotary Engine (RENESIS)," SAE Technical Paper 2004-01-1790, 2004, doi:10.4271/2004-01-1790.
40. I. Gamma Technologies. [Online]. Available: https://www.gtisoft.com/. [Accessed Jan 2015].
41. Wimmer A., Skriptum: Thermodynamik des Verbrennungsmotors (Block 9), Graz: TU Graz: Institut für Verbrennungskraftmaschinen und Thermodynamik, 2012.
42. Weberbauer F., Rauscher M., Kulzer A., Knopf M. und Bargende M., "Allgemein gültige Verlustteilung für neue Brennverfahren," Motortechnische Zeitschrift, MTZ 2/2005 Jahrgang 66, 2005.
43. Golloch R., Downsizing bei Verbrennungsmotoren, Berlin Heidelberg: Springer-Verlag, 2005, ISBN 3-540-23883-2.
44. Bargende M., Burkhardt C. und Frommelt A., "Besonderheiten der thermodynamischen Analyse von DE- Ottomotoren," Motortechnische Zeitschrift, MTZ 62 (2001) 1, 2001.
45. Ebner H. W. und Jaschek A. O., Die Blow-by-Messung - Anforderungen und Meßprinzipien, Motortechnische Zeitschrift 59, 1998.
46. Wimmer A., Skriptum: Thermodynamik des Verbrennungsmotors (Block 10), Graz: TU Graz: Institut für Verbrennungskraftmaschinen und Thermodynamik, 012.

Contact Information

Felix Zahradnik
felix.zahradnik@ifa.tuwien.ac.at

Johann Spreitzer
johann.spreitzer@ifa.tuwien.ac.at

Vienna University of Technology
Institute for Powertrains & Automotive Technology
Getreidemarkt 9
A-1060 Vienna

The Engineering Meetings Board has approved this paper for publication. It has successfully completed SAE's peer review process under the supervision of the session organizer. The process requires a minimum of three (3) reviews by industry experts.

All rights reserved. No part of this publication may be reproduced, stored in a retrieval system, or transmitted, in any form or by any means, electronic, mechanical, photocopying, recording, or otherwise, without the prior written permission of SAE International.

Positions and opinions advanced in this paper are those of the author(s) and not necessarily those of SAE International. The author is solely responsible for the content of the paper.

ISSN 0148-7191

http://papers.sae.org/2015-01-0382